MIR-pump NIR-probe fiber-optic photothermal spectroscopy with background-free first harmonic detection

CHENYU YAO,[1] SHOUFEI GAO,[2,3] YINGYING WANG,[2] PU WANG,[4] WEI JIN,[3] AND WEI REN[1,*]

[1]*Department of Mechanical and Automation Engineering, The Chinese University of Hong Kong, New Territories, Hong Kong SAR, China*

[2]*The Institute of Photonics Technology, Jinan University, Guangzhou 510632, China,*

[3]*Department of Electrical Engineering, The Hong Kong Polytechnic University, Kowloon, Hong Kong SAR, China*

[4]*Beijing Engineering Research Center of Laser Technology, Institute of Laser Engineering, Beijing University of Technology, Beijing 100124, China*
Corresponding author: renwei@mae.cuhk.edu.hk

Abstract: We demonstrated MIR-pump NIR-probe photothermal spectroscopy with the first harmonic (PTS-1f) detection of formaldehyde, one of the most common volatile organic compounds (VOCs), in a silica hollow-core negative curvature fiber (HC-NCF). The photothermal gas sensor adopts a mid-infrared interband cascade pump laser at 3.6 μm and a near-infrared fiber probe laser at 1.56 μm. At the optimal modulation frequency (8 kHz) and modulation index (1.8) of the pump laser, we obtained a normalized noise equivalent absorption (NNEA) coefficient of 4×10^{-9} cm^{-1}WHz$^{-1/2}$. The use of HC-NCF with an inner diameter of 65 μm enables the sensitive photothermal detection even for a very low pump power of micro-watts. The background-free PTS-1f detection was observed to enhance the sensitivity by a factor of 2.4 compared to the second harmonic (2f) detection. A theoretical model was established in this work to interpret the experimental results.

1. INTRODUCTION

Photothermal spectroscopy (PTS) is a highly sensitive trace gas sensing technique which typically uses a pump-and-probe configuration [1,2]. The pump laser causes the localized heat generation via gas absorption, which induces the change of the refractive index (RI) in the gas medium. A probe laser propagating through the same region undergoes a phase shift that can be detected by an optical interferometer. To enhance the detection sensitivity, PTS has been recently performed in a hollow core fiber (HCF) with a tiny cross section to obtain an extraordinarily large light intensity over a long distance [3,4]. Jin et al. [3] pioneered the development of an ultra-sensitive C_2H_2 sensor (2 ppb) with an ultra-wide dynamic range (>10^5) by performing the near-infrared (1.56 μm) pump-probe detection in a hollow-core photonic crystal bandgap fiber (HC-PBF).

Instead of the near-infrared (NIR) wavelength region, many gas molecules have much larger absorption cross-sections in the mid-infrared (MIR) region between 3 μm and 12 μm due to the strong rovibrational resonance in the fundamental band. To take advantage of the MIR molecular fingerprint region, we recently proposed the MIR-pump NIR-probe PTS for trace gas detection in HCFs [5,6]. In this novel pump-probe configuration, the use of a MIR-pump laser enables the more efficient localized heating even with a low incident laser power. Rather than measuring the direct absorption using expensive MIR HgCdTe (MCT) photodetectors, the

probe laser detection makes use of commercially available NIR detectors operating at room temperature. Additionally, the use of an HCF as a gas cell significantly reduces the sample volume of the target analyte.

In PTS, the periodic heating of the sample relies on a modulated pump laser by using amplitude modulation (AM) or wavelength modulation (WM). The amplitude modulation of laser intensity could be realized by implementing external modulators (i.e., mechanical chopper and acoustic optical modulator) [7,8] or amplitude-modulated laser sources [9]. The wavelength modulation, another widely used method in PTS, could be accomplished by sinusoidally modulating the injection current of a tunable semiconductor laser [8,10]. A lock-in amplifier is normally adopted to extract the second harmonic ($2f$) component of the detection signal.

It should be noted that the sinusoidal modulation of the injection current of semiconductor lasers produces the simultaneous modulation of laser frequency and intensity. The resultant laser intensity modulation is often referred to as residual amplitude modulation (RAM). If the transmitted laser after gas absorption is detected by a photodetector (i.e., wavelength-modulation absorption spectroscopy) and demodulated exactly at the modulation frequency (first harmonic or $1f$), the RAM gives rise to a strong background signal superimposed by a weak gas absorption [11,12]. As an indirect laser absorption technique, PTS detects the gas absorption by an optical interferometer using the probe laser. In the pump-probe detection scheme, the RAM of the pump laser has negligible contribution to the non-absorption background of the probing interferometer. Hence, the magnitude of $1f$ signal could be directly obtained without the need for background subtraction [13,14]. It is of interest to know that the $1f$ signal has the largest magnitude among all the harmonic components of wavelength modulation.

In this work, we demonstrated MIR-pump NIR-probe PTS of formaldehyde, which is one of the most common volatile organic compounds (VOCs), at 3.6 µm with the $1f$ detection of wavelength modulation. A silica hollow-core microstructured fiber was used as the gas cell for the pump-probe detection. The wavelength modulation parameters of the interband cascade pump laser were examined to obtain the highest signal-to-noise ratio (SNR) for the $1f$ detection. The influence of the pump and probe powers on the photothermal detection was also investigated. Finally, a theoretical model was proposed to interpret the experimental results, as well as to examine the zero-background nature and the influence of RAM on the PTS-$1f$ signal.

2. EXPERIMENTAL METHODS

Fig. 1 depicts the experimental setup of PTS-$1f$ detection of formaldehyde in a hollow-core negative curvature fiber (HC-NCF). An interband cascade laser (ICL) emitting at 3.6 µm was used as the MIR pump laser to exploit the Q(7) line at 2778.48 cm^{-1} in the ν_1 fundamental band of formaldehyde. HC-NCF is attracting many research groups due to its simple geometry, broad spectral bandwidth and low transmission loss [15-17]. The recently developed silica HC-NCF with nearly single-mode transmission in the MIR region was used as the gas cell for PTS detection. Such a HC-NCF has a hollow-core inner diameter of 65 µm inscribing by a single ring of six nontouching silica capillaries (see the inset graph in Fig. 1); and more details of this fiber could be found elsewhere [18, 19]. The ICL of 1.6-mW pump power was coupled into the HC-NCF by a CaF$_2$ lens (focal length, 50 mm). The 120-cm long HC-NCF was coiled by a radius of 15 cm to reduce the system size; and negligible bending loss was observed.
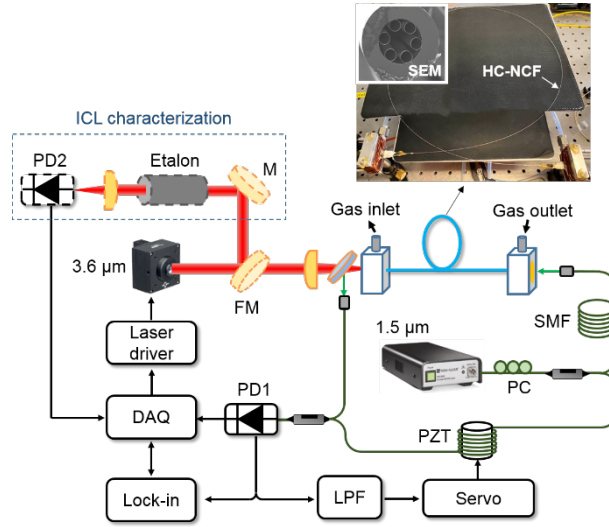
Fig. 1. Experimental setup of MIR-pump NIR-probe photothermal spectroscopy of formaldehyde in a HC-NCF. FM: flipped mirror; M: plane mirror; LDC: laser diode controller; PD1: NIR photodetector; PD2: MIR photodetector; PC: polarization controller; SMF: single mode fiber; DAQ: data acquisition; LPF: low pass filter. Inset: photo of the coiled HC-NCF along with a scanning electron microscope (SEM) image of the fiber cross-section.

The HC-NCF also serves as one arm of a Mach-Zehnder interferometer (MZI) for the photothermal phase detection using a NIR probe laser at 1.56 μm, as illustrated in Fig. 1. The phase modulator in the other arm locks the MZI at the quadrature point by compensating the ambient noise. The MZI signal is detected by a NIR photodetector followed by the wavelength-modulation $1f$ detection using a lock-in amplifier. As a demonstration, the HC-NCF was filled with the formaldehyde/nitrogen mixture (0.55 bar) with a certified concentration of 30 ppm at room temperature.

The ICL was modulated at a relatively high frequency (f, kHz) and also slowly scanned (mHz) across the absorption line by varying the electrical voltage applied to the laser driver. To characterize the tuning characteristics of the ICL such as the wavelength modulation depth, a flip mirror was placed in the optical path to direct the laser beam through a germanium etalon (free spectral range, FSR = 0.0164 cm^{-1}) onto a MCT photodetector (PD2 in Fig. 1). It should be noted that such a laser characterization process is only used for the theoretical modeling analysis to be discussed in Section 4; and thus PD2, etalon and the relevant optics are not required for the actual photothermal detection.

A typical characterization process is demonstrated in Fig. 2 by applying an 8-kHz sinusoidal modulation with an amplitude of 225 mV. The wavelength modulation and RAM of the ICL depicted in Fig. 2 are well fitted by the sinusoidal functions. A phase shift of 1.09π between the wavelength modulation and RAM is observed. Here we define the modulation index, m, as the ratio of the modulation depth to the half-width at half-maximum (HWHM) of the absorption line. At the gas pressure 0.55 bar, m was measured to be 1.8 for the present modulation settings. The modulation index could be adjusted by varying the modulation voltage.
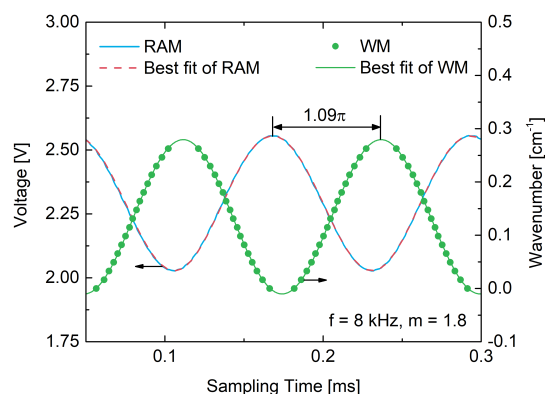
Fig. 2 Representative RAM and WM of the ICL for a sinusoidal modulation (8 kHz, 225 mV) applied to the laser driver.

3. RESULTS

All the measurements were performed for 30 ppm formaldehyde at 0.55 bar. Fig. 3(a) depicts the representative PTS-1f signals measured at different modulation indexes in the wavelength range from 2777.8 cm^{-1} to 2779.2 cm^{-1}. The injection current of the ICL was modulated by a sinusoidal waveform at 8 kHz and simultaneously ramped by a 100-mHz sawtooth. The corresponding absorption spectrum of formaldehyde simulated using the HITRAN database [20] is plotted in Fig. 3 (b). The PTS-1f signal approaches zero at the far wing of the measured spectrum, indicating the background-free nature of PTS-1f detection. By adjusting the sinusoidal voltage applied to the laser driver, it is of interest to observe in Fig. 3(a) that the peak-to-peak amplitude and the peak-to-peak spectral distance vary with the modulation index.
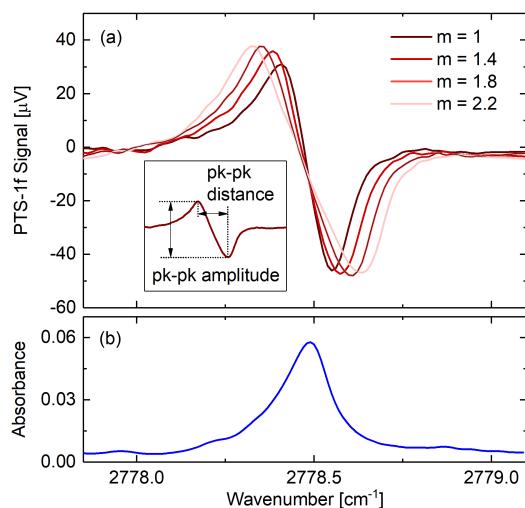

Fig. 3. (a) Representative PTS-1f signals of 30 ppm formaldehyde (P = 0.55 bar) measured at the fixed modulation frequency (8 kHz) and the varied modulation indexes. (b) Simulated absorption spectrum based on the HITRAN database.

Fig. 4 plots the peak-to-peak amplitude and spectral distance of the PTS-1f signal as a function of modulation index. At a higher modulation index, the PTS-1f signal generally

becomes stronger and broader. The spectral distance between the two peaks of the 1*f* signal increases almost linearly with the modulation index. The optimal modulation index was found to be around 1.8, corresponding to the largest amplitude of 1*f* signal.
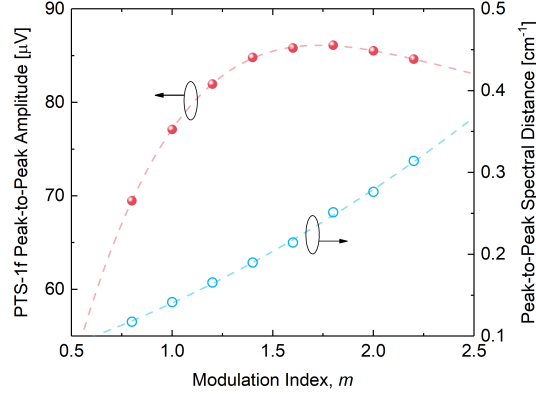

Fig. 4 Variation of peak-to-peak amplitude and spectral distance of PTS-1*f* signal (30 ppm formaldehyde, 0.55 bar) with the modulation index.

As the 2*f* detection is usually adopted for PTS, it is of interest to compare these two detection methods. Fig. 5(a) depicts the typical 1*f* and 2*f* harmonic signals at the modulation index 1.8 and modulation frequency 8 kHz. The measured peak-to-peak amplitudes at different modulation frequencies between 2 kHz and 12.5 kHz are plotted in Fig. 5(b). In general, a larger 1*f* signal is observed at a lower modulation frequency. Note that the relatively small PTS-1*f* signal at the modulation 2 kHz is probably caused by the low-pass filter (1 kHz) used for the MZI phase locking. The PTS-1*f* signal is observed to have a larger amplitude than that of the 2*f* signal by a factor of 2. Meanwhile, the background signal obtained by measuring pure nitrogen is also plotted in Fig. 5(b) for comparison. The noise level (1σ) of the PTS-1*f* detection is generally larger than that of the 2*f* detection because of the 1/*f* flicker noise and other slowly-varying noise in the ambient. However, such a difference in noise becomes negligible for these two detection schemes at a modulation frequency larger than 6 kHz.
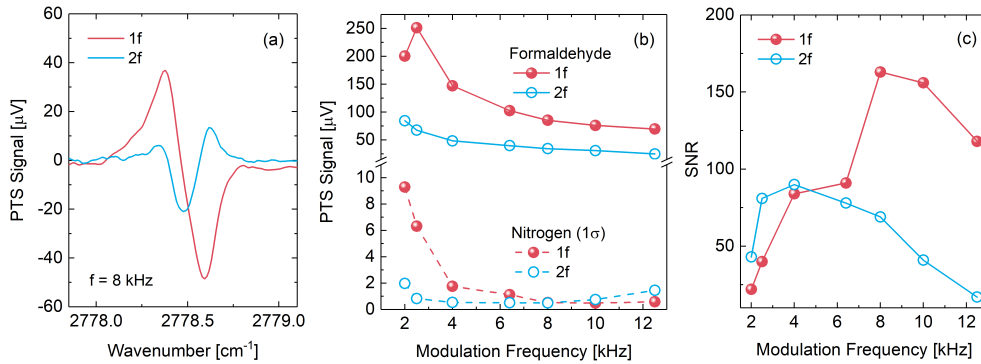

Fig. 5. (a) Representative PTS-1*f* and 2*f* signals for 30 ppm formaldehyde at 0.55 bar. (b) Variation of PTS-1*f* and -2*f* measurements with the modulation frequency of the ICL pump laser. (c) Comparison of the SNR of PTS-1*f* and 2*f* measurements.

Finally, Fig. 5(c) compares the SNR of the PTS-1f and 2f detection schemes over the modulation frequency from 2 kHz to 12.5 kHz. A larger SNR of PTS-1f detection is evident when the modulation frequency is selected larger than 6 kHz. In particular, the optimal modulation frequency is identified to be around 8 kHz, where the 1f detection improves the SNR by a factor of 2.4 compared to the 2f detection. By achieving a detection SNR of 163 for 30 ppm formaldehyde, we estimate a minimum detection limit (MDL) of 0.18 ppm in this work, corresponding to a normalized noise equivalent absorption (NNEA) coefficient of 4×10^{-9} cm^{-1}WHz$^{-1/2}$.

We also investigated the influence of pump and probe powers on PTS-1f detection. Fig. 6(a) shows the representative PTS-1f signals under different pump powers. The peak-to-peak amplitude of the PTS-1f signal at each pump power is plotted in Fig. 6(b) along with the corresponding noise level by measuring nitrogen filled in the HCF. The PTS-1f signal increases linearly with the MIR pump power, whereas the background noise (1σ) keeps almost unchanged. Additionally, the present photothermal sensor can be operated at a very weak pump power due to the strong absorption cross-section in the mid-infrared and the high power density in the tiny hollow core fiber. For instance, the sensor was able to capture the signal of 30 ppm formaldehyde with a SNR of 9 for a pump level of 60 μw. It should be noted that the photothermal gas detection has seldom been demonstrated at μw-level pump power previously.
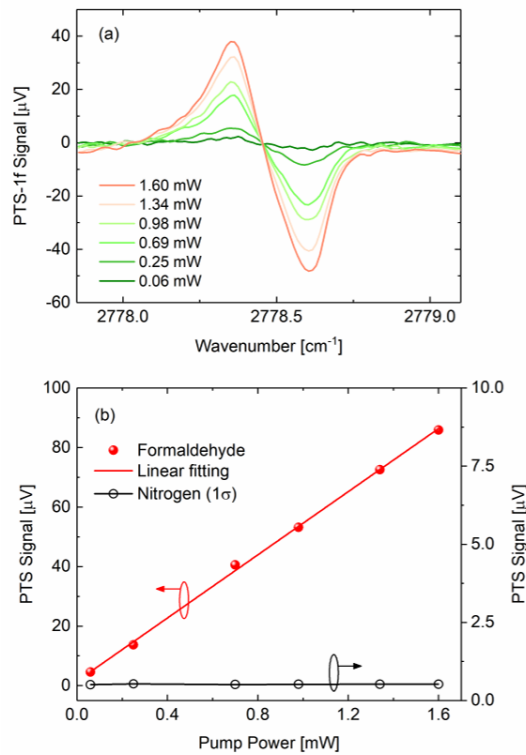

Fig. 6. (a) Representative PTS-1f signals measured at different pump powers. (b) Variation of PTS-1f measurements with the pump power.

Additionally, Fig. 7(a) compares the PTS-1f signals at different NIR probe powers. The gain of the NIR photodetector was adjusted accordingly to maintain a stable interferometric voltage level. At the fixed pump power of 1.6 mW, negligible difference is observed among these measurements using different probe powers. Fig. 7(b) plots the peak-to-peak amplitude

and noise level with the probe power varied between 40 µW and 4 mW. Hence, the photothermal phase detection is insensitive to the probe power.
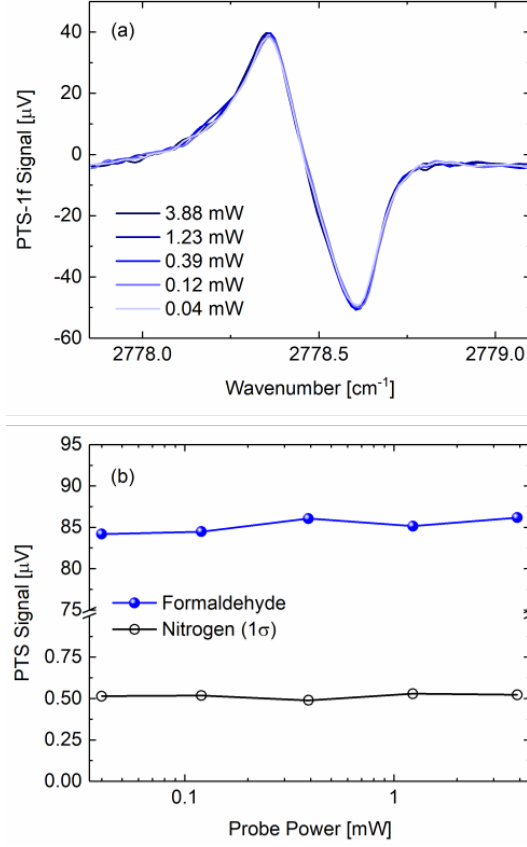

Fig. 7 (a) Representative PTS-1f signals of 30 ppm formaldehyde measured at different probe powers; the pump power is fixed at 1.6 mW. (b) Variation of PTS-1f measurements with the NIR probe power.

4. DISCUSSION

To interpret the experimental data and understand the detection mechanism, a theoretical model of wavelength-modulation PTS-1f detection is described here. The wavelength modulation of the MIR pump laser can be expressed as:

$$v(t) = v_0 + a \cdot \cos(2\pi ft),\qquad (1)$$

where v_0 (cm^{-1}) is the center wavelength of the laser under modulation, and a(cm^{-1}) is the modulation depth. The modulation of the injection current of the pump laser also produces a simultaneous intensity modulation, known as the RAM:

$$I_{pump}(t) = I_0 \cdot \left[1 + \sum_{n=1}^{\infty} i_n \cdot \cos(n \cdot 2\pi ft + \theta_n)\right],\qquad (2)$$

where I_0 is the average laser intensity at v_0, i_n is the nth-order Fourier coefficient of intensity modulation, and θ_n is the corresponding phase shift. Note that the high-order components ($n > 2$) of the intensity modulation could be ignored for most semiconductor lasers.

The photothermal effect is directly related to the local heat production rate (H) caused by gas absorption of the pump laser [3]:

$$H = Y_H \cdot k(v) \cdot I_{pump},$$ (3)

where Y_H is the heat yield and k(cm^{-1}) is the absorption coefficient. Such a periodic heating process changes the refractive index of the gas inside the hollow core fiber, thus leading to the phase change $\Delta\varphi$ of the NIR probe laser. For a small $\Delta\varphi$, the MZI linearly converts the phase change into the intensity change ΔS:

$$\Delta S = G \cdot \alpha(v) \cdot I_{pump},$$ (4)

where G is the proportional coefficient and $\alpha(v)$ is the spectral absorbance of the target gas. Since the pump wavelength is sinusoidally modulated, the resultant spectral absorbance can be expanded in Fourier series:

$$\alpha\left[v_0 + a \cdot \cos(2\pi ft)\right] = \sum_0^\infty H_k(v_0, a) \cdot \cos(k\omega t),$$ (5)

where H_k is the amplitude of the kth harmonic component. Therefore, the wavelength-modulation 1f signal can be expressed by:

$$S_{1f} = \frac{GI_0}{2} \cdot \left[H_1 + i_1 \cdot \cos\theta_1 \cdot \left(H_0 + \frac{1}{2}H_2 \right) + i_2 \cdot \cos\theta_2 \cdot \left(\frac{1}{2}H_1 + \frac{1}{2}H_3 \right) \right].$$ (6)

It is evident in Eqn. (4) that the PTS-1f signal is directly proportional to the absorbance α. In wavelength-modulation absorption spectroscopy, however, the fractional transmission ($e^{-\alpha}$) introduces a large non-absorption background signal [21,22], which is directly inherited from the i_1-component of RAM in the transmission and significantly affects the 1f signal. In contrast to absorption spectroscopy, the PTS-1f detection avoids the direct detection of the transmitted light and hence is background-free; in fact, the signal is dominated by the first Fourier harmonic component (H_1) of the absorbance. It should be noted that the RAM may slightly affect the spectral profile of the PTS-1f signal shown in Eqn. (6).

Based on the theoretical PTS-1f model, Fig. 8 compares the simulated PTS-1f signals with the measurements at two different modulation indexes; the fitting residuals are plotted at the bottom panel. A full list of laser modulation parameters used in the model is provided in Table 1. Note that the PTS-1f signal is normalized by the peak-to-peak amplitude for a fair comparison. It is evident that the theoretical calculation agrees better with the measurement when the RAM is considered in the model; the fitting residual is generally within 3% shown in Fig. 8. However, the additional RAM has negligible effect on the non-absorbing region at the far wing of the measured spectrum, thus confirming the background-free nature. In fact, the RAM only slightly distorts the spectral profile but has little influence on the peak-to-peak amplitude, because the i_1-component of Eqn. (6) consist of H_0 and H_2 which are symmetric functions of wavenumber around the absorption line center.

Table 1. Characterization of the 3.6 μm ICL

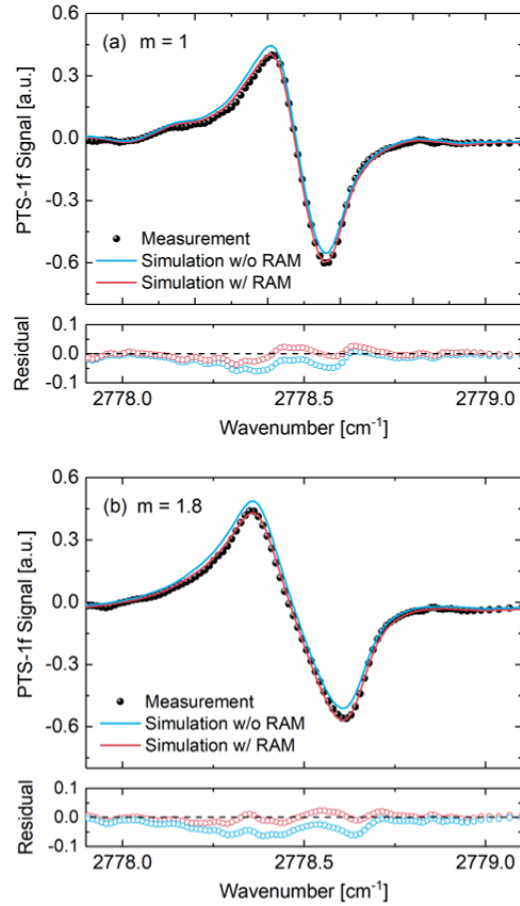| Sinusoidal modulation	a/cm^{-1}	m	i_1	θ_1	i_2	θ_2
8 kHz, 125 mV	0.080	1.0	0.056	1.09π	0.0007	1.49π
8 kHz, 225 mV	0.145	1.8	0.100	1.09π	0.0017	1.29π

Fig. 8. Comparison of the measured PTS-1f signal with the simulation of 30 ppm formaldehyde (0.55 bar) at different modulation indexes: (a) $m = 1.0$, and (b) $m = 1.8$.

As previously illustrated in Fig. 4, the PTS-1f signal becomes broader and larger for a larger modulation index. We performed the detailed simulation of the PTS-1f signals at different modulation indexes shown in Fig. 9. The peak-to-peak amplitude reaches a plateau level when the modulation index m is greater than 1.6. The good agreement between the measurement and the simulation indicates the PTS-1f measurement can be well predicted by the current model. However, we ignored the influence of the modulation frequency in this work. In fact, the modulation frequency affects the ICL tuning characteristics and is also associated with the thermal dynamics of the photothermal phase modulation and the hollow-core fiber geometry [23].
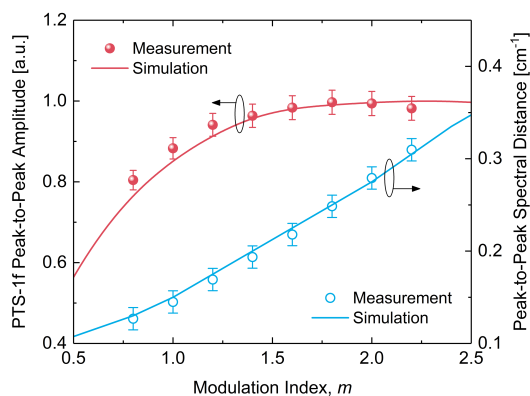
Fig. 9. Comparison of the measured and simulated PTS-1f peak-to-peak amplitude and spectral distance as a function of the modulation index.

5. CONCLUSION

In conclusion, we have demonstrated MIR-pump NIR-probe photothermal spectroscopy of formaldehyde using the 1f detection of wavelength modulation. Formaldehyde was detected by employing a 3.6 µm ICL as the pump source. A silica HC-NCF with a length of 120 cm and a hollow core of 65 µm was used as the gas cell. The fiber was coiled by a radius of 15 cm to reduce the sensor size but with a negligible bending loss. The sensor performance was optimized at the modulation frequency 8 kHz and the modulation index 1.8, leading to a detection limit of 0.18 ppm formaldehyde and NNEA coefficient of 4×10^{-9} cm^{-1}WHz$^{-1/2}$. The PTS-1f signal is proportional to the pump power but is insensitive to the variation of probe power. A detection SNR of 9 was obtained for a pump power of 60 µW. Moreover, the PTS-1f method improves the sensitivity by a factor of 2.4 compared to the conventional 2f detection. A theoretical model was built in this work to interpret the PTS-1f measurement, further verifying its background-free nature and minimally affected by the RAM of the pump laser.

REFERENCES

1.   C.C. Davis, S. J. Petuchowski, Appl. Opt. **20**, 2539 (1981).
2.   M. A. Owens, C. C. Davis, R. R. Dickerson, Anal. Chem. **71**, 1391 (1999).
3.   W. Jin, Y. Cao, F. Yang, H. L. Ho, Nat. Commun. **6**, 1 (2015).
4.   P. Zhao, Y. Zhao, H. Bao, H. L. Ho, W. Jin, S. Fan, S. Gao, Y. Wang, P. Wang, Nat Commun. **11**, 847 (2020).
5.   Z. Li, Z. Wang, F. Yang, W. Jin, W. Ren, Opt. Lett. **42**, 3718 (2017).
6.   C. Yao, Q. Wang, Y. Lin, W. Jin, L. Xiao, S. Gao, Y. Wang, P. Wang, W. Ren, Opt. Lett. **44**, 4048 (2019).
7.   Y. Lin, W. Jin, F. Yang, J. Ma, C. Wang, H. L. Ho, Y. Liu, Sci. Rep. **6**, 1 (2016).
8.   K. Krzempek, G. Dudzik, K. Abramski, G. Wysocki, P. Jaworski, M. Nikodem, Opt. Express **26**, 1125 (2018)
9.   A. Totachawattana, H. Liu, A. Mertiri, M. K. Hong, S. Erramilli, M. Y. Sander, Opt. Lett. **41**, 179 (2016).
10. J. P. Waclawek, C. Kristament, H. Moser, B. Lendl, Opt. Express. **27**, 12183 (2019).
11. P. Kluczynski, O. Axner, Appl. Opt. **38**, 5803 (1999).
12. K. Chen, S. Liu, L. Mei, F. Jin, B. Zhang, F. Ma, Y. Chen, H. Deng, M. Guo, Q. Yu, Analyst. **145**, 1524 (2020)
13. Z. Yang, G. Yin, C. Liang, T. Zhu, IEEE Photonics J. **10**, 7102307 (2018).
14. C. Roller, A. Fried, J. Walega, P. Weibring, F. Tittel, Appl. Phys. B. **82**, 247 (2006).
15. M. H. Frosz, P. Roth, M. C. Günendi, P. St.J. Russell, Photon. Res. **5**, 88 (2017).

16. F. Tani, F. Köttig, D. Novoa, R. Keding, P. St.J. Russell, Photon. Res. **6**, 84 (2018).
17. S. Gao, Y. Wang, W. Ding, D. Jiang, S. Gu, X. Zhang, P. Wang, Nat. Commun. **9**, 2828 (2018).
18. L. Cao, S. Gao, Z. Peng, X. Wang, Y. Wang, P. Wang, Opt. Express. **26**, 5609 (2018).
19. C. Yao, S. Gao, Y. Wang, P. Wang, W. Jin, S. Member, W. Ren, J. Light. Technol. (2019), DOI: 10.1109/JLT.2019.2960804.
20. I. E. Gordon, L. S. Rothman, C. Hill, R. V Kochanov, Y. Tan, P. F. Bernath, M. Birk, V. Boudon, A. Campargue, K. V Chance, B. J. Drouin, J.-M. Flaud, R. R. Gamache, J. T. Hodges, D. Jacquemart, V. I. Perevalov, A. Perrin, K. P. Shine, M.-A. H. Smith, *et al.*, J. Quant. Spectrosc. Radiat. Transf. **203**, 3 (2017).
21. G. B. Rieker, X. Liu, H. Li, J. B. Jeffries, R. K. Hanson, Appl. Phys. B Lasers Opt. **87**, 169 (2007).
22. H. Li, G. B. Rieker, X. Liu, J. B. Jeffries, R. K. Hanson, Appl. Opt. **45**, 1052 (2006).
23. H. Bao, Y. Hong, W. Jin, H. L. Ho, C. Wang, S. Gao, Y. Wang, P. Wang, Opt. Express. **28**, 5423 (2020).